J. Plasma Physics (2013), vol. 79, part 3, pp. 273–285. © Cambridge University Press 2012
doi:10.1017/S0022377812000967

High-speed imaging of dust particles in plasma

C. M. TICOŞ[1,2], D. TOADER[2], M. L. MUNTEANU[2], N. BANU[2] and A. SCURTU[2]

[1]National Institute for Research and Development in Microtechnologies, Bucharest 077190, Romania (catalin.ticos@inflpr.ro)
[2]National Institute for Laser, Plasma and Radiation Physics, Bucharest 077125, Romania

(Received 20 April 2012; revised 23 August 2012; accepted 11 October 2012; first published online 19 November 2012)

Abstract. High-speed imaging is a powerful tool for studying dusty plasmas. The recorded trajectories of dust particles can provide direct information about the physical processes involved in dust-plasma and dust–dust interactions. A review of some experiments and their imaging techniques employed for tracking dust particles immersed in low-ionized gases and in high-density plasma jets is presented. Digital cameras are used to record the motion of slow or hypervelocity dust particles dragged by plasma jets, or to evidence single or collective dust particle oscillations and vibrations in the plasma sheath.

1. Introduction

The exponential increase in the speed of electronic circuitry, particularly of data processing and especially the advent of the charge-coupled device (CCD), and its continuous improvement over the years have paved the way for the successful fabrication of image-recording devices that once seemed only to be a subject of science fiction (Boyle and Smith 1970). Not long ago, perhaps 30 years ago or so, researchers struggled with film cameras; however, they invented clever techniques to capture fast evolving processes. Of course, the camera itself was not the whole story but nevertheless it proved to be invaluable in their work, leading to many breakthroughs in all fields of sciences from biology to physics or chemistry. An example is the bubble chamber (the Wilson chamber) used in detecting charged nuclear particles. The first nuclear explosions were also high-speed photographed on film to review all the stages of shock wave propagation. Nowadays, film cameras may still appeal to art photographers, but the incontestable more versatile CCD or Complementary metal-oxide-semiconductor (CMOS)-based cameras have become the rule in all imaging applications. The advantages are evident: electronic recording and storage, instantaneous access to data, high resolution, real-time control and synchronization capabilities which go beyond the nanosecond threshold, and last but not least, blazing frame rates. State-of-the-art video cameras have unprecedented capabilities and can record fast events at 1 million frames per second (fps).

High speed cameras are a must-have tool in the study of dusty plasmas. Among many optical diagnostics, high-speed imaging has emerged as one of the most powerful techniques suitable to track the trajectories of small objects. Plasmas filled with such small entities, hence the name 'dusty', are perfect candidates for such detailed exploration. Dusty plasmas are often called complex plasmas due to their intricate structure: a collection of charged ions or molecules, electrons, fields and particles of matter. This last component differentiates dusty plasmas from all other types of plasmas and confers them some unique properties. It is probably why the research of dusty plasmas has picked up in the last 15 to 20 years to become one of the most prolific branches of plasma physics in terms of scientific output (Shukla and Mamun 2002).

Size-wise, there is a difference of many orders of magnitude between the constituents of plasmas, i.e. the atomic particles (neutrals, electrons, and ions) and the particles of matter or dust particles which can be made up of a few atoms or of billions of atoms and reach hundreds of microns in size. As an example, the mass of an electron is 9.1×10^{-28} g, that of an argon ion is 6.7×10^{-23} g, while that of a plastic dust grain with 5 μm in diameter is about 10^{-11} g. The complex nature of dusty plasmas is fully understood when we consider interaction between all the constituents (Shukla and Eliasson 2011). There are short-range interactions, such as head-on collisions or long-range interactions of the Coulomb type. It is important to understand that in a system with free electrical charges, the dust grains themselves end up charged electrically. Electrons and positive ions collide with a dust grain and are trapped on its surface. The charging process is continuous and sustained by streaming electrons and ions from the surrounding plasma. The negative or positive charges either accumulate or neutralize each other. The net charge at a given moment of time is a result of dynamic equilibrium between the fluxes of electrons and ions on the dust surface (Kennedy and Allen 2003). The flow of charges is mediated by local potentials, which give rise

https://doi.org/10.1017/S0022377812000967 Published online by Cambridge University Press

to electric fields. The electric potential of a dust grain establishes the density of nearby electrons and ions but is also intermediating the interaction with other electrically charged particles of matter. The dust particles can be made in principle of any material and can have any structure. Dust can be inserted in plasma or can be formed in specific conditions. The presence of gases, such as silane, methane, or acetylene, favors dust particle to grow from small agglomerates of several tens of nanometers to a few microns (Hayashi 1999; Cavarroc et al. 2008). In practice, these dust particles can have various shapes, from perfect spheres to approximately round, elongated, or just completely irregular. Individual or collective particles' motion can be tracked to infer useful information about the evolution and dynamics of dusty plasma as a whole.

In this paper we plan to review the application of high-speed cameras in low-temperature dusty plasmas and in high-density dusty plasma jets. We discuss the performance of several imaging techniques depending on the requirements imposed by the physical system under study. While in experiments with static dust particles, a low frame rate of only 20–30 fps is often sufficient, for hypervelocity dust particle exposures of a few microseconds is essential to capture some meaningful physical parameters. Emphasis will be put on a few of the most interesting findings based on direct observations of dust trajectories.

In the first section, the main issues concerned with the imaging of plasma crystals and slow-moving dust are approached. Here the advantages or drawbacks of the techniques concerned with imaging collective motion of particles in the context of using single or multiple cameras are discussed. In the next section, the requirements for real-time tracking dust flying at speeds of a few meters per second and the challenges for optimum dust capture are reviewed. Finally, in the last section it is described how detection of microparticles moving in plasma at very high speeds of a few kilometers per second is realized. When the size of the dust particles is not known *a priori*, a simple technique for inferring the diameter of a dust particle captured in a frame is presented. Concluding remarks about the use of high-speed cameras and future experiments are drawn at the end.

2. Tracking dust particles in plasma

One can generally divide detection of dust particles in plasmas in two categories, depending on dust motion features: slow and fast moving dust. Coincidentally, this classification generally corresponds to the types of plasmas where dust is resident: thin and weakly ionized plasmas or dense and highly ionized plasmas. In the first category, the dust particles have a relatively slow motion of a few millimeters per second or at the most several centimeters per second and their trajectories are somewhat easy to monitor. For these less dynamic dust particles one CCD camera is typically the standard requirement in the simplest experiments for recording the projection of dust trajectory on one plane, vertical or horizontal (Chu and Lin 1994; Thomas et al. 1994; Trottenberg et al. 1995; Fortov et al. 1996; Pieper et al. 1996; Merlino et al. 1997; Law et al. 1998; Samsonov et al. 2000; Samarian et al. 2001; Thomas 2001; Ticos et al. 2003; 2004a, b, c). Frame rates of cameras, which prove to be sufficient for these types of applications, vary for those affordable which run at 25 fps to over 500 fps for more expensive equipments. Within this range, CCDs with megapixel resolution are quite common at acceptable prices and fit well in the relatively small budget of a dusty plasma experiment.

In sophisticated experiments dedicated to imaging of a large number of dust particles which aim to build statistics of some physical quantities such as dust temperature, several techniques can be employed. Particle image velocimetry (PIV) is used to infer vector fields of the particles' motion when the dust number densities are sufficiently high such that individual particles cannot be resolved (Thomas 2006). Single camera systems, which are rather 2D systems and can only image the motion projected onto the laser sheet, cannot satisfy the need to gain insight into the three-dimensional (3D) structure of a dust cloud. More evolved techniques used in tracking flows have been borrowed for the diagnostics of dusty plasmas (Willert and Gharib 1991). Stereoscopic PIV using two CCD cameras has been employed by Williams and Thomas (2007) to depict the kinetic velocity space distribution for 3.11 μm MF and 1.51 μm silica particles in a DC plasma. The dust temperature T_d was inferred by fitting the distribution curve with a Maxwellian. For pressures in the range of 100–130 mtorr, T_d was larger than the electron temperature by a factor of 10. By operating three or even four cameras, the three spatial components of dust speed over an extended plasma volume could be measured (Williams 2011). CCD cameras with 14 bit and 1648 $\times$ 1214 pixel resolution were used.

Particle tracking velocimetry (PTV) is another technique which uses multiple cameras to measure simultaneously the 3D position and motion of particles. Structural and dynamics investigations of a Yukawa ball made of spheres with a diameter of 3.46 μm have been carried out using stereoscopic PTV with two and three cameras, respectively (Block and Melzer 2010). The third camera in the later case could help identify the overlapping particles in images recorded at frames rates of up to 100 fps. A PTV method based on holography was introduced by Piel et al. (2008) with the purpose of resolving dust trajectories at micron level by using a video-microscope to record interference patterns in the scattered light off a dust cloud. The holograms are read to reconstruct the 3D position of each particle. A key requirement is a high-resolution image (4 Mpixels) to contain the fine details of interference fringes. This

https://doi.org/10.1017/S0022377812000967 Published online by Cambridge University Press

technique seems more suitable for static particles, with a low number density, and with a relatively large size ($\gtrsim$10 μm) to insure adequate contrast. The slow frame rate at which holograms are recorded (tens of frames per second) is at present a disadvantage.

Refining and improving the imaging tools has led to a large quantity of data to be processed during or after an experiment. New algorithms based on a matrix algorithm (Himpel et al. 2011) or using a Kalman filter for tracking shocked dust (Oxtoby et al. 2012) have been developed.

The most critical parameter of a high-speed camera is perhaps its frame rate. This has to be chosen carefully on the basis of experimental needs. As an example, if one observes dust particles oscillating at 20 Hz, then according to the Nyquist sampling criterion one should videotape the trajectory at a frame rate of at least 40 fps. In practice a much higher frame rate is used, of a few hundred frames per second to catch all the infinitesimal details of the trajectory, as they can give important clues about the forces acting on the particle. The exposure time is another important parameter in high-speed imaging of dusty plasmas. It intervenes especially when fast moving particles are in the field of view. In many situations the exposure is set as the inverse of the frame rate, which means that between consecutive frames the shutter is continuously open and the intensity of each pixel builds up in time. In order to avoid streaking of dust trajectories, the exposure can be progressively reduced until only a short section of the path traveled by the particle is caught in each frame. There is always a tradeoff between exposure and luminosity, i.e. the shorter the exposure, the darker the frame. This disadvantage can be overcome by using more powerful lasers to illuminate dust particles.

The optics of a high-speed camera is as important as the CCD itself. To be able to observe particles of a few microns in size at several tens of centimeters, a good close-up lens is required. Nikon, Canon, and other optics companies offer a wide range of lenses, an example being the Micro-Nikkor 60 mm F/2.8 D. In high-density plasma jets, the dust particles can move much faster, with speeds in the range from tens or hundreds of meters per second to several kilometers per second. Much more sophisticated and therefore more expensive cameras are needed to capture snapshots of dust trajectories. Some examples are the DicamPro used at Los Alamos in plasma fusion experiments (Wang et al. 2007), the PCI 1024 FastCam, the Kodak Motion Coder, and Phantom cameras used in tokamaks experiments (Roquemore et al. 2007; Rudakov et al. 2008). Since in these experiments the dust particles are relatively far from the camera, at distances between tens of centimeters to meters, only powerful telephoto zoom lenses can focus and produce images of submillimeter particles. An example of affordable telephoto lens is the Sigma 50-500 mm f/4.5-6.3.



Figure 1. Side view of a plasma crystal.

3. Plasma crystals

Plasma crystals are entities in which the particles occupy specific positions in space, or, in other words, the spatial distribution of dust particles in a given plasma volume is periodic. The particles self-arrange until the forces acting on themselves cancel out and a particular distance between each other is established, closely related to plasma parameters, the dust particles size, and the charging state of the particles. Typical parameters are: dust radius $\approx$ 1 to 15 μm and distance between particles = 200–700 μm. The symmetry of such entities is either BCC or FCC, but generally the two coexist (Pieper et al. 1996). The realization of this type of particles arrangement at this size and time scale has proved to be particularly useful for studying in real time the fundamental properties of crystals, and it is of great importance for basic physics research. An example of plasma crystal is presented in Fig. 1. Here perfect spheres made of melamine formaldehyde (MF) with a diameter of 6.03 μm hover in the plasma sheath of a radio-frequency (RF) plasma. Plasma crystals have so far been observed in low ionized gases such as RF plasmas (Chu and Lin 1994; Thomas et al. 1994), DC discharges (Fortov et al. 1996), and in Q-machines (Merlino et al. 1997).

A prerequisite for obtaining such 3D periodic dust structures in the laboratory is to insure that the plasma Debye length is a few times larger than the size of the particles, or $\lambda_D > r_d$. This condition allows for long-range Coulomb dust–dust interactions. A parameter which is generally used to define the formation of crystals is the coupling factor Γ, defined as the ratio of electrostatic energy of interaction between two adjacent particles and their kinetic energy. When $\Gamma \geqslant 70$, the particles are strongly coupled and self-organization of the particles into periodic structures is possible (Ikezi 1986). For Debye lengths $\lambda_D < r_d$, the particles are screened from each other by plasma electrons and ions and any mutual interaction is prevented. The system with weakly or non-interacting dust grains is also called 'dust in plasma', rather than dusty plasma. This last situation is often encountered in much more dense plasmas of tokamak reactors, dense plasma jets, etc. While dust is associated with these types of plasmas, no crystals have been observed so far. An experimental set up for trapping and confining dust crystals in an RF plasma is presented in Fig. 2. Plasma is produced between two parallel plate electrodes placed a few centimeters apart. The bottom electrode is coupled to an RF high-

https://doi.org/10.1017/S0022377812000967 Published online by Cambridge University Press

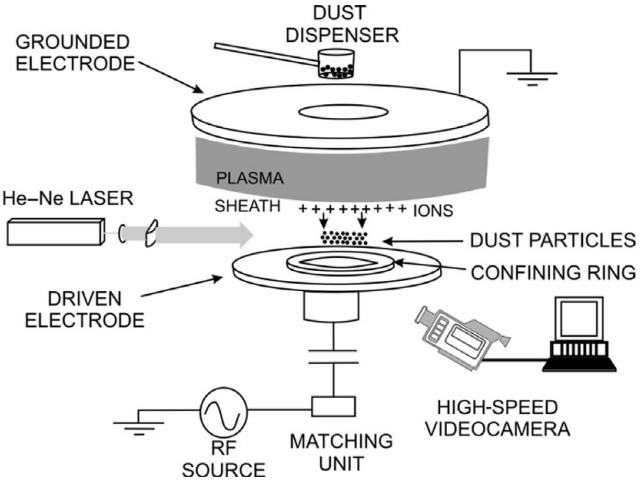


Figure 2. Typical experimental set up for trapping and monitoring dust particles in RF plasma.

voltage source, which can deliver a few hundred volts at 13.56 MHz, while the top electrode is usually grounded. Dust particles released in the plasma are trapped inside the sheath of the bottom electrode, as seen in Fig. 1. A ring is placed on the electrode to confine dust particles to a limited region viewed by a high-speed camera.

The parameters of an RF plasma in which 'crystallization' of dust particles is possible are as follows: $n_e \sim 10^{14}$ to 10^{16} m^{-3}, $T_e \sim 1$ to 5 eV, and argon gas pressure, $P \approx 150$–400 mtorr. Some interesting phenomena can be observed when the gas pressure is lowered. The kinetic energy of dust particles increases since the drag of the neutral gas weakens and the crystal starts 'melting'. The process is local, as shown in Fig. 3, and initially the crystalline and 'melted' regions alternate, with the last one eventually spreading to the whole crystal when the pressure is further lowered (Thomas and Morfill 1997). The transition from crystal to liquid phase is well predicted by theory and confirms the experimental findings (Melzer et al. 1996). In the so-called 'liquid' phase, the dust particles have a random oscillatory motion about a fixed position. The coupling parameter also decreases about two orders of magnitude, close to 1. At even lower pressure, the dust particles have a Brownian motion, and the dust cloud resembles a fluid in gaseous phase. For obtaining the images of Fig. 3, a Micro-Nikkor 60 mm f/2.8D lens was mounted on the CCD camera. A set of three spacers with a total length of 68 mm was put between the lens and the CCD detector to bring the focusing distance closer, down to ≈13 cm. Also, a teleconverter ×2 was added for increased magnification leading to a resolution of 72 pixels/mm in the images with 1024 × 1024 pixels. The horizontal section in the plasma crystal shows equal spacing between dust particles with a hexagonal symmetry at a neutral gas pressure of 383 mtorr. At 216 mtorr, some particles are oscillating with amplitudes roughly equal to the separation distance between the particles of ≈470 μm.

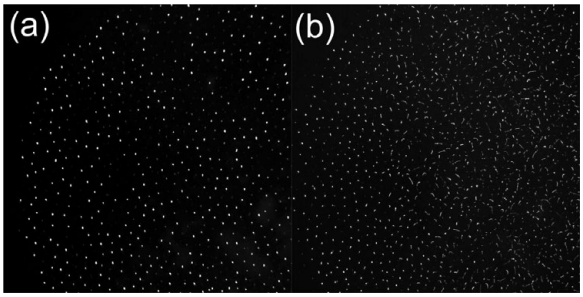


Figure 3. (a) Horizontal section in a plasma crystal, and (b) 'crystalline' and 'liquid' states coexisting in a dust cloud at a lower gas pressure.

Uchida et al. (2009) have shown that a beam of electrons streaming through dust particles can trigger phase transition from liquid to crystalline state by bringing dust particles together. The electron beam was obtained from an auxiliary discharge, while the particles were spheres with 10 μm diameter.

It has been discovered that by placing a dielectric box (e.g. a cube with 3-cm side) on top of the RF electrode plasma, crystals in the shape of a perfect sphere or 'Coulomb balls' could be created in this new type of confinement. The symmetry of such a structure is hexagonal with defects to allow for the curvature of the shell (Arp et al. 2004). One key feature of the experimental set up is the conducting coating (indium tin oxide) applied on the surfaces of box walls, which is transparent and allows a clear view of dust cloud inside the box.

4. Collective motion of dust particles

The main forces acting on dust particles are the electric force of the sheath field, the gravity force, the neutral drag exerted by collisions with the neutral atoms of gas, the Coulomb force of neighboring particles, and the ion drag exerted by ion flow in the sheath. Dust particles are put in motion when the resultant force acting on them is non-zero. The first three forces are dominant in low ionized gases such as those produced in a laboratory set up. The radiation force or the electron pressure are weak and have no significant impact on dust dynamics. The ion drag force arises from the flux of positive plasma ions interacting with the negatively charged grain. There are two contributions to the ion drag force: the direct impact force of ions collected by the dust particle and the long-range Coulomb force, when ions passing nearby transfer a fraction of their momentum to the dust particle, without however touching its surface (Barnes et al. 1992; Khrapak et al. 2002; Hutchinson 2005). A stream of ions directed at a dust particle can be focused behind it and create spatial varying potential wells, the so-called wake potential (Lapenta 2002). Particle-in-cell (PIC) simulations have proved that modification in the local potential due to positive charge accumulation downstream a dust particle can exert attraction for other dust particles found nearby. The local potential can be

https://doi.org/10.1017/S0022377812000967 Published online by Cambridge University Press

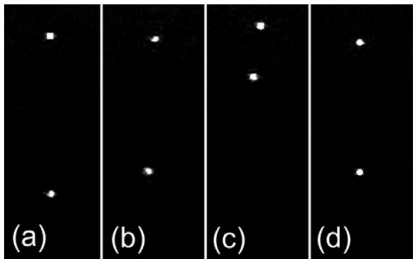


Figure 4. (a) to (b): Oscillations of vertically aligned dust particles with a diameter of 13.7 μm. The bottom particle being attracted toward the upper one.

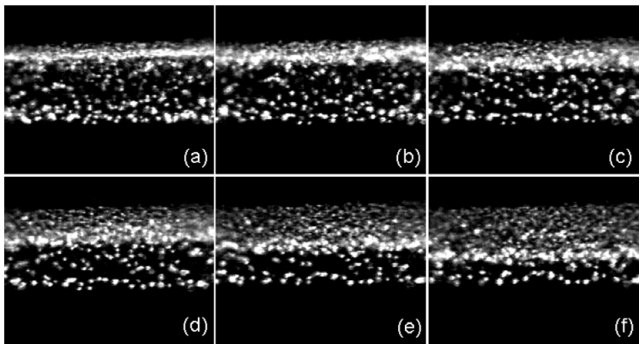


Figure 5. Vertical propagation of dust density waves from top (a) to bottom (f) of a dust crystal levitated in plasma. The height of the crystal is 1.7 mm.

of $\approx 0.5\ V_d$, where V_d is the dust potential. This is the case in the situation presented in Fig. 4, which shows the oscillation of a dust particle in the wake of another identical particle, both of them floating in the plasma sheath (Ticos et al. 2003, 2004c). Ions flowing from the plasma to the lower electrode through the sheath create behind the top dust particle an attractive wake potential for the bottom particle. Thus, the particle is put in motion and climbs up into the sheath until the repulsive Coulomb force exerted by the top particle slows it down. The particle falls and regains its initial lower position. The process then repeats itself indefinitely. The phenomenon was observed within a narrow range of gas pressures, i.e. from 44 to 46 mtorr. The gas pressure was a key parameter in this experiment; it established not only the strength of the neutral drag force but also the mean free path of ions in the sheath. It appears that for these pressures all the conditions were met for an optimum focusing of the ion beam and creation of the attractive wake potential. The gas drag seemed to be sufficiently weak to not dissipate the kinetic energy gain which led to the oscillatory motion of dust particles. The images in Fig. 4 were recorded at 250 fps by a NAC HSV 500 digital camera provided with a Pentax FA 100-mm macro zoom lens. The resolution was about 57 pixels/mm.

The transition from a vertical to a horizontal string in a system with two particles of a few microns in diameter, trapped in the RF plasma sheath, has been studied by Samarian et al. (2005). The oscillating regimes and the equilibrium states have been mapped in the space spanned by the peak-to-peak RF voltage (from 20 to 80 V) and neutral gas pressure (between 20 and 50 mtorr). The particles were recorded at a resolution of 640×480 pixels and frame rates of up to 100 fps. Longer vertical strings made of eight melamine particles with 8.89 μm diameter were excited by Kong et al. (2011) at different frequencies between 1 Hz and 20 Hz with an external sine wave.

5. Dust waves

Collections of a large number of dust particles are easily driven out of equilibrium due to an external action, especially considering that the particles are electrically charged. The equilibrium is fragile due to mutual interactions between grains but also due to interaction with the surrounding plasma. Nevertheless, there are factors that work favorably for establishing a state of minimum kinetic energy when the repulsion forces are equilibrated. One is the neutral gas drag. The friction of dust particles with gas atoms is proportional to the gas pressure and dust speed, when the last is low compared with the gas thermal speed. There are also factors that drive the dust cloud out of stability, such as the ion flow. Positive ions flow from the plasma to the electrode, streaming through dust particles. Their trajectories are affected by the negatively charged dust particles creating locally a net spatial positive charge. As a result the dust particles align vertically and occupy these attractive potential well, leading to the formation of vertical strings. On the other hand, the energy of streaming ions can induce dust particle motion. The ion–dust streaming instability has a gas pressure threshold below which collective dust oscillations are triggered (Rosenberg 1996). The dust particles oscillate in phase and the dust wave propagates from one end of the dust cloud to the other (Mamun and Shukla 2011). Dust acoustic waves (DAW) were predicted theoretically by Rao et al. (1990) and first observed experimentally by Chu et al. (1994) in an RF magnetron system and by Barkan et al. (1995) in a Q-machine. Images of waves propagating in a plasma crystal are shown in Fig. 5. This self-induce instability is sustained by incoming ions and the relaxation time is set by the inertia of dust particles. The typical frequency of this type of dust waves is of the order of 20–30 Hz, with phase speed of a few centimeter per second. Depending on the dust number density and the strength of the dust-dust coupling, wave beating phenomena and propagation of oblique dust waves relative to the direction of ion flow in the sheath can be observed. In Fig. 5 the waves were recorded at 250 fps with an image size of 210×110 pixels and a resolution of 56 pixels/mm. The measured phase speed of the waves was 1.96 cm/s. The waves propagated in a crystal formed from perfect plastic spheres with a diameter of 3.4 μm (Ticos et al. 2004b).

Plasma crystals confined by a metallic ring or by a cut in the electrode consists of about 15 to 20 horizontal

https://doi.org/10.1017/S0022377812000967 Published online by Cambridge University Press

layers. By levitating the dust cloud inside a conducting box placed on top of an RF electrode, crystals with many more layers can be produced (Flanagan and Goree 2010). Triggering the waves by lowering the argon pressure below 426 mtorr has allowed the observation of waves propagating at 24–26 Hz over the longer vertical extent of the crystal of 4 mm. In this experiment, MF spheres with a diameter of 4.8 μm were tracked with a 12-bit CCD camera at 500 fps in a rectangle of 273×404 pixels. The resolution was 76.4 pixels/mm. Dust-acoustic waves have been observed recently in a DC plasma in front of the anode. The waves produced in a dust cloud with an average dust diameter of 1 μm self-steepened and collided eventually (Heinrich et al. 2009). Recordings of the crest waves propagating at 20 cm/s and with a frequency of 54 Hz have been carried out at 500 fps with a 1-Mpixel video camera Photron Fastcam-1024 PCI. The dust acoustic oblique waves propagating at a large angle relative to the direction of ion flow and with a phase velocity of 2 cm/s have been tracked at 100 fps in a microgravity experiment and with a resolution of 1280×640 pixels (Piel et al. 2008). Solitons were launched in a 2D plasma crystal made of particles with a diameter of 9.19 μm by biasing a pair of wires placed in-between the RF electrode and crystal (Harvey et al. 2010). The collision of two oppositely traveling solitons was captured with a camera at 500 fps and resolution of 1024×1024 pixels.

6. Falling dust

When the equilibrium of dust particles becomes unstable and the electric force becomes weaker, the particles fall to the electrode due to the force of gravity (Ticos et al. 2004a). An instance when this phenomenon happens is presented in Fig 6. Here the RF plasma is perturbed by a plasma jet propagating parallel with the RF electrodes. The jet was produced inside a miniature coaxial plasma gun. Although the density of the plasma jet was about an order of magnitude higher (10^{16} m^{-3}) than that of RF plasma, the highly drifting electric charges of the jet moving axially with a few kilometers per second affected the ionization processes in RF plasma. It appears that sustainment of RF plasma was strongly perturbed. Thus, for a short period of time the RF plasma shut down and reinstated itself when the perturbation was removed. The initial electric sheath field which insured the equilibrium of the plasma crystal was lost as well when the RF plasma was turned off. Since there was no electric force to equilibrate the force of gravity, all the particles forming the plasma crystal had a downward vertical trajectory as shown in the images of Fig. 6. Here the exposure time was set at 33 ms and the frame rate was 30 fps. Interestingly, after the perturbation has been removed, the RF plasma was turned on and the electric sheath field built up again. Some of the dust particles which were on their way toward the bottom electrode were again subjected to electric force and their falling

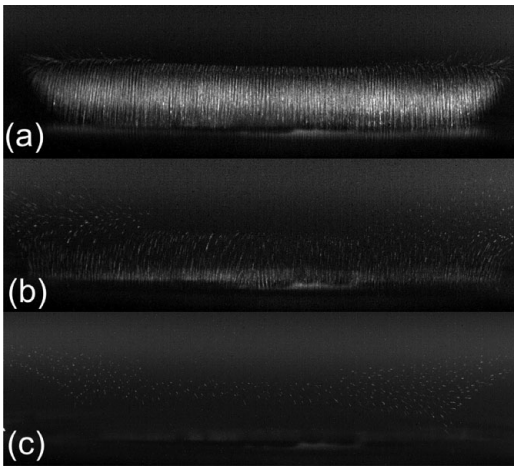


Figure 6. (a) and (b) Falling of a dust crystal when the RF plasma is temporarily perturbed; (c) rearrangement of dust particles.

trajectory had changed direction, becoming an ascending one. The dust particles moved around inside the sheath until they reached a stable position where all forces cancelled out. The sheath electric field was perpendicular only at the center of the confining zone. Toward the edge of it, the field lines were curved, resulting in a non-zero horizontal component of electric force acting on dust particles. This situation is reflected in the image by the presence of particles moving at an angle with the local vertical axis.

A similar situation was observed in the dusty plasma after-glow (Layden et al. 2011). After switching off the RF plasma, the floating dust particles kept a residual charge and eventually fell to the electrode with a speed which depended on the bias applied on the electrode. Their falling trajectories were recorded at 500 fps. The particles were grown inside the plasma and illuminated with a thin laser sheet.

7. Dragged dust particles in plasma

Dust particles can be easily pushed by a stream of charged particles, such as ions, given their relatively small mass. The requirement is that the applied force of ion drag overcomes the opposed forces of friction with the neutral gas or the electrical or gravitational forces acting on the dust particle. An experiment where trapped dust particles in RF plasma were pushed out of the trapping region has been carried out (Ticos et al. 2010a, b). A plasma jet consisting of drifting ions and electrons was produced in a few centimeters long coaxial plasma gun. The coaxial gun was inserted inside the vessel of RF plasma. The gun had two electrodes: a center rod and a coaxial outer cylindrical shell, both made of stainless steel. The muzzle of the gun was at about 5 mm from the RF electrode (see Fig. 7). The electrodes were powered from a capacitor charged up to 2 kV by a high-voltage power supply. The inter-electrode gap was filled with the gas present inside the chamber

https://doi.org/10.1017/S0022377812000967 Published online by Cambridge University Press

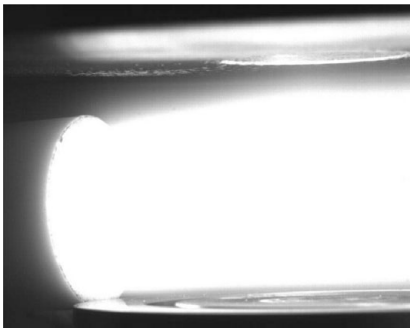


Figure 7. Plasma jet produced in a coaxial gun entering between the electrodes of an RF plasma.



Figure 8. (a) to (d): Plasma jet propagation in time at different applied voltages on coaxial gun: 800, 1000, 1500 and 2000 V, respectively.

of RF plasma at the same pressure of about 265 mtorr. The jet was fired by closing a high-speed current switch. The measured peak currents of the discharge produced in the coaxial gun were between 10 A and 23 A. The jet produced near the dust crystal found at rest in the confining potential of the RF electrode is shown in Fig. 7. In this image, the exposure time was set at 8 ms, while the frame rate was 125 fps.

In order to infer the speed of the jet, a long section of about 256 × 16 pixels along the propagation direction was monitored at a much higher frame rate of 73,000 fps and an exposure of 13.7 μs. The jet displacement for different discharge voltages of the coaxial gun, between 800 V and 2000 V, is shown in Fig. 8 . The plasma jet speed was found to be between 2 km/s and 4 km/s.

The particles were dragged above the RF electrode on almost linear trajectories, as shown in Fig. 9. The images were captured with the Photron Fastcam PCI 1024 and a lens provided with a set of three spacers (68 mm in length) and a teleconverter 3×. The camera speed was 3000 fps with an exposure of 0.33 ms. The particles were illuminated with a laser sheet obtained by passing the beam of a diode laser with 15 mW emitting at 650 nm through a cylindrical lens. A red filter centered at the laser wavelength was put in front of the camera lens for filtering out plasma light.

The long dust traces are due to relatively long exposure time, comparable to the time required for microparticles to cross a large part of the view area. The drag force acting on the particles is proportional to the plasma density n_i, the ion mass m_i, the dust radius r_d, the thermal speed of ions v_{ti}, and a function G(s), where $s = v_{fi}/v_{ti}$,

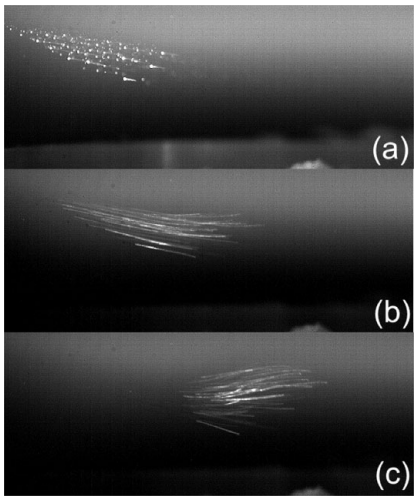


Figure 9. (a) to (c): Dragged dust particles by a focused plasma jet in an RF dusty plasma.

with v_{fi} the plasma flow speed: $F_{\text{coll}} = n_i r_d^2 m_i v_{ti} G(s)\sqrt{\pi}/2$. Here the drag force F_{coll} is a direct impact force which accounts for the ions collected on the surface of dust particles. Setting trapped dust particles in motion by firing a short pulsed plasma jet could be in principle a useful technique for removing dust.

It is well known that dust accumulates in plasma processing reactors which use specific gases in capacitive RF discharges. The particles grow in time from tens of nanometers to several tens of microns, up to the point where their weight cannot be sustained anymore by the electric force of sheath field. At the end of the process when the plasma is turned off, the formed dust particles fall on the processed surface and destroy it. Other methods of dust removal are based on laser pushing of dust particles, neutral gas dragging, or on electrostatic traps (Schill 2002; Kurimoto et al. 2004). The density of the plasma jet produced in our experiment appeared to be strong enough to effectively drag all the floating dust particles. In our case electron drag is negligible due to low electron mass. For the pulse duration of our experiment of a few millisecond, the plasma jet density was in the range 10^{16}–10^{17} m^{-3}, one or two orders of magnitude higher than that of RF plasma.

Directed ion flows are usually present in the sheath of a plasma when ions are accelerated to electrodes. An interesting situation appears when the discharge takes place in microgravity conditions, at pressures between 50 mtorr and 450 mtorr. Since the force of gravity acting on the particles is negligible, these are not anymore confined to a limited region near the electrode and eventually fill up the entire discharge except its central region, which is left empty of dust. Ions streaming from the center of the discharge drag dust particles along toward the edge of the plasma. The dust cloud finds its equilibrium when the ion drag and the electric forces compensate each other, resulting in a plasma crystal with a large void free of particles. It has been observed that when two different size particles are present in the discharge,

https://doi.org/10.1017/S0022377812000967 Published online by Cambridge University Press

they do not mix with each other. Small dust particles (1 to 3 μm) released inside the void of a dusty plasma go through the empty spaces between larger particles (of up to 14 μs in diameter) forming strings which move radially as if they had a predetermined lane to go on, as demonstrated by Sütterlin et al. (2009). Two CCD cameras operating at a maximum 50 fps were used to image the dust cloud.

An alternate method to manipulate dust particles in plasma is using the action of termophoretic force $\propto \nabla T_n$, where T_n is the temperature of neutral atoms of gas. The increase in the temperature of the nearby gas can generate a strong vertical gradient such that dust particles are pushed upward and act as massless (Arp et al. 2004). The temperature can be tunned to give rise to a termophoretic force equal to the force of gravity. The pressure of photons coming from a laser beam with a power of tens of mW can also push particles out their equilibrium position (Melzer 2001). A short laser pulse can create compressional waves of a few tens of Hertz which propagate through the crystal.

8. Hypervelocity dust in dense plasma jets

Solid particles of matter present in a specific environment, such as a moving fluid, are strongly influenced in terms of motion and mutual interaction. In liquids and gases, fluid viscosity plays a determining role in microparticle dynamics. Although it is one order of magnitude weaker in gases than in liquids, the viscous force can still entrain dust particles in a gas flow. This remarkable property of sampling the flow is widely used in PIV (Adrian 1991; Willert and Gharib 1991; Lindken et al. 2006). By extension, electrically charged fluids, such as plasmas, can put in motion dust particles and some of the plasma properties can be deduced indirectly by observing dust trajectories. However, the plasma density as well as the flow speed need to be sufficiently high to induce an observable effect. The conditions are fulfilled in high-density plasma jets created in powerful coaxial guns. A dense plasma jet was produced in a powerful 200-MW coaxial plasma gun fired from a 50-kJ capacitor bank charged at a maximum 10 kV. The discharge was triggered by switching a water-cooled ignitron. The pulse duration was of the order of 300 to 400 μs. Up to 250 kA of electric current was passing through the inter-electrode space ionizing in high proportion the filled gas, which in our case was deuterium, for compatibility with fusion applications (Ticos et al. 2006b). The ions were ejected at speeds between 40 km/s and 60 km/s by the $\mathbf{J} \times \mathbf{B}$ force, where $\mathbf{J}$ is the current density flowing between coaxial electrodes and $\mathbf{B}$ is the magnetic field from Ampere's law. The coaxial gun length was about 70 cm, while the spacing between the center rod and the outer cylindrical electrode was 15 mm. An image of the jet was captured by a DicamPro ICCD camera with gating capabilities down to 5 ns and is shown in Fig 10. The image had

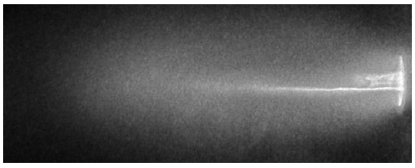


Figure 10. Image with microsecond exposure of a dense plasma jet.

an exposure of 1μs and was recorded at 50 μs from time zero of the discharge. The diameter of the jet was about 20 cm and its length shown in the image was about 75 cm. The jet was launched in a large cylindrical vacuum vessel and imaging was possible from a window positioned at the end of the vessel. Both discharge and camera were triggered by a digital pulse generator. The timing of the camera was adjusted to properly account for jet propagation inside the coaxial channel and connecting flanges, which were about 1.4 m in length. A fish eye lens with 16 mm f/4 was mounted on the camera. Contrast and gain of the camera were adjusted to avoid overexposure due to the intense emission of plasma. Fine details of the jet structure could be observed in the recorded image indicating the presence of bright filaments swirling along the propagation direction, with lengths of the order of several centimeters (Ticos et al. 2011).

Dust particles were sprinkled at mid-length of the coaxial gun from a container shaken by a piezoelectric transducer. The container was mounted on a flexible bellows and could store up to a few grams of powder. Microparticles made of carbon (graphite and synthetic diamond) with diameters from 1 to 48 μm and 40 to 60 μm, respectively, acquired from commercial suppliers were used. At the interaction with plasma, the dust particles were dragged in the direction of the jet. The dominant force acting on the dust particles was the direct impact ion drag force, a few orders of magnitude higher than the electric force or the gravity force. The long-distance Coulomb force was negligible as the dense plasma would screen the charged dust particles, with the Debye length being only of few microns (Ticos et al. 2006a). The acceleration of a dust particle was of the order of 10^6–10^9 m/s^2 leading to a speed of up to 4 km/s achieved over a distance of only 1 m (Ticos et al. 2008a, b). An illustration of flying microparticles dragged by the plasma flow is presented in Fig. 11. The image had an exposure of 14 μs and was acquired 700 μs after firing of the gun. The ion and electron temperatures were relatively low in the plasma jet, up to 10 eV; however, the dense plasma particle fluxes colliding with dust particles would heat them up. In comparison with the case of low ionized gases, the dust particles were self-illuminated and emitted light due to their high temperature. Their detection in this respect was different in the sense that although no laser beam was needed to illuminate the microparticles, a much faster camera was required to track them.

https://doi.org/10.1017/S0022377812000967 Published online by Cambridge University Press

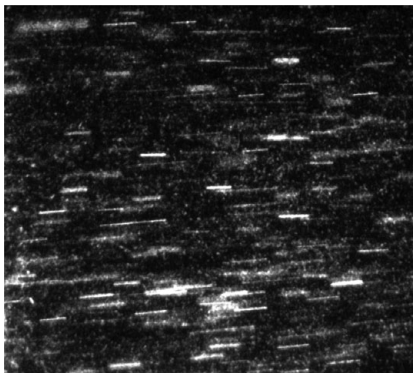


Figure 11. Hypervelocity dust storm with particles moving at speeds between 0.2 km/s and 3 km/s.

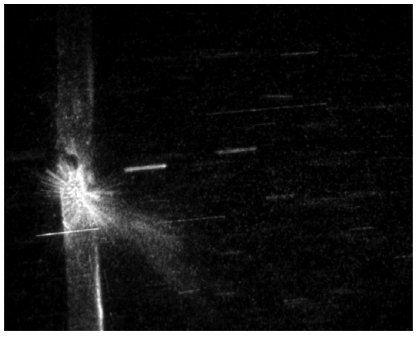


Figure 12. Hypervelocity dust particles colliding with a stainless steel sheet.

At hypervelocity speed, the time of flight over a distance equal to the camera's field of view is very short, i.e. of a few microseconds. A simple estimation gives the exposure time for a field of view of 1 cm and a speed of 1 km/s: $t_{exp} = 10^{-2}/10^{3} \approx 10^{-5}$s. Thus, an exposure of the order of tens of microseconds is needed. In our case, the field of view has been chosen relatively large, of several centimeters, while the exposure time was set at values between 4 μs and 16 μs. The traces of the particles moving with different speeds had different lengths, as can be easily seen in Fig. 11. In a more spectacular image, the impact of a dust grain with a stainless steel (SS) sheet has been captured, as presented in Fig. 12. The initial dust particle broke into many smaller pieces, which flew in opposite directions with speeds from a few tens to hundreds m/s. Other dust particles flying at different speeds were seen to miss the SS sheet and continued their motion. Their traces had different widths, corresponding to different dust diameters. The exposure of the image was 12 μs obtained at 500 μs after igniting the plasma jet. A telephoto lens with 500 mm f/4 was employed to magnify a region of about 12 $\times$ 14 cm, situated about 1.6 m downstream from the gun muzzle.

9. Imaging of large dust particles

In not all cases, the dust size is *a priori* known. For example, dust particles formed inside the fusion plasma by erosion of the machine wall during its interaction with the hot plasma can have in principle any size ranging from hundreds of nanometers to hundreds of microns (Roquemore et al. 2007; Rudakov et al. 2008). These small pieces of material are then transported by plasma flows at different locations and can possibly hit or cover some equipment parts such as antennas, probes, or the divertor, affecting their proper functioning. Monitoring their trajectories can be carried out using high-speed cameras. These microparticles are usually heated by the plasma at high temperatures and glow by themselves in the visible spectrum. However, even when they are detected, not much information is obtained about their structure and shape. Their size can be approximated by knowing the capabilities of the optical system used for imaging.

In most cases dust in fusion plasmas is viewed as an unwanted by-product. While at present it is not of much concern, in the next-generation tokamaks, such as ITER, accumulation of large quantities of dust will potentially pose a bigger threat. One of the threats is the risk of radioactive contamination of activated dust particles which contain nuclei of tritium. On the other hand, dust could play an important role for local diagnostics (Wang et al. 2006). Dust with known properties released inside a magnetically confined plasma produced in a tokamak can be used to map local magnetic field lines. The plume resulted from the ablation of microparticles by hot plasma is normally oriented along the magnetic vector. A large number of such particles launched synchronously can therefore provide information about the direction of field vectors over a sufficiently large volume, up to the limit where the presence of dust starts to induce perturbations in the plasma. As a matter of fact, experiments with dust particles injected inside fusion plasma have already been undertaken with Lithium Deuteride (LiD) dust particles in the NSTX reactor (Nichols et al. 2011). Another example where dust can play a useful role comes from the imaging of 3D plasma flows.

Fluorescent dust particles were released inside a large coaxial gun, at the Flowing Magnetized Plasma Experiment (FMP) of Los Alamos (Wang et al. 2007). The facility consisted of a 60-cm diameter coaxial gun powered from a bank of capacitors charged up to 900 V, with a total energy of 100 kJ. The ultraviolet (UV) emission of the He plasma discharge was intense and excited the dust material, which in turn emitted in the visible range. The dust particles could be observed without additional laser illumination as is the case with most of the low-density plasma experiments, and without heating from the plasma as seen in fusion plasmas. Two identical Dicam Pro ICCD cameras with exposures set at 400 μs were triggered simultaneously. Up to five consecutive frames could be recorded by cameras, hence the pearl-like aspect of a moving dust particle in seen Fig. 13.

On each camera telescopic lenses of f = 500 mm were used. The cameras had roughly perpendicular views. The

https://doi.org/10.1017/S0022377812000967 Published online by Cambridge University Press

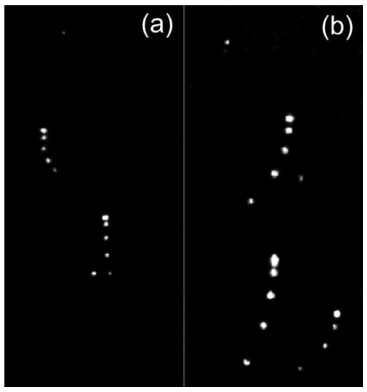


Figure 13. 3D dust motion in the FMP experiment: (a) Axial view, and (b) side view with trajectories along radial direction.

two dust particle trajectories seen in the image with axial view are the same as presented in the image with side view. While the used powder was made of particles of 5 μm in diameter, the detected dust particles were much larger with sizes of a few hundred microns. This was due to high adhesion and clumping together of many particles. In our experiment the dust dispenser based on a piezoelectric shaker could not release single micro particles, but rather larger dust chunks. This situation is different from typical experiments with plasma crystals where small particles of a few microns are observed (Feng et al. 2007).

In spite of their large mass, the falling trajectories of dust particles were bent in the direction of the plasma flow. The plasma parameters were: flow speed 15 km/s, plasma density $\sim 10^{19}$ m^{-3}, and ion and electron temperatures of 10 to 15 eV. The flow was however 3D, swirling about the longitudinal axis of the coaxial gun. This feature was reflected in dust trajectories. The measured dust accelerations in the axial and radial directions agreed well with the value predicted by a model for ion drag force. The dust charge was established by the flowing currents to the dust surface. The ion current was obtained in the sheath-limited theory, considering a thin sheath surrounding the perfect dust sphere, comparable with the Debye length. In order to evaluate the force acting on a spherical dust particle, the value of the radius was needed. It was deduced from correlating the radius of the bright spot corresponding to the particle in the recorded image with the parameters of the optical system which depended on the wavelength, the limited diffracted spot, the focal lens, and the pixel size of CCD. The intensity of pixels in the image of a dust particle shown in Fig. 14 along horizontal and vertical directions is represented in two graphs. Each section passes through the brightest pixel in the image. A Gaussian fit on both x and y axes is performed.

The dust particle diameter was taken at 10% of the maximum peak intensity. In the 256 bits images, the most luminous pixel had an intensity, $I_{\max} = 256$ relative to a completely dark pixel ($I_{\min} = 0$), therefore the boundary defining the particle corresponded to the

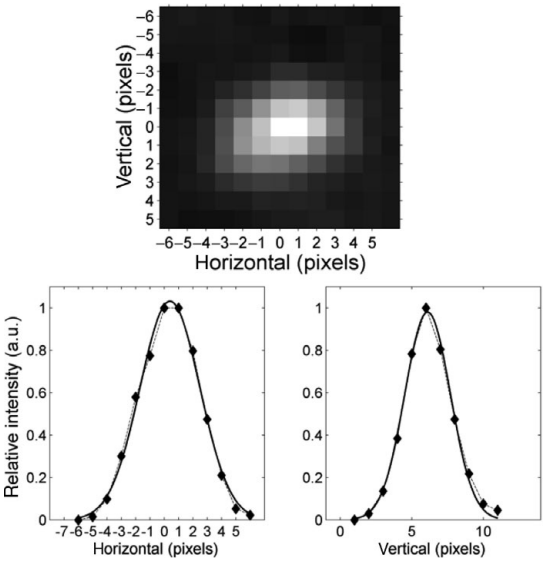


Figure 14. Image of a microparticle at pixel resolution, and fits of brightness in the vertical and horizontal sections through image center.

intensity, $I_d \approx 26$. The particle was considered spherical, and in the plane of the image the particle diameter was taken as $d_d \approx \sqrt{d_{dx}^2 + d_{dy}^2}$, where d_{dx} and d_{dy} were the measured diameters along the two perpendicular axes: $d_d \approx 6.78$ pixels. The ICCD of the Dicam Pro had a pixel size of 6.7 $\times$6.7μm. The actual dust radius was then, $r_d = \sqrt{d_d^2 - d_s^2}/2M$, where $d_s = 2.44(1 + M)\lambda f\#$ was the diffraction limited spot diameter for the camera with a lens magnification, $M = 4$. The center wavelength was at $\lambda = 560$ nm, while $f\# = 2.2$. Most dust particles were found to have a radius in the range 100 to 200 μm. The individual dust particle radii were about 10 to 20 times the Debye length, which was $\sim$10 μm for flowing plasma produced in the experiment. In our case ($r_d \gg \lambda$) the image of the particle approaches the geometrical limit and is approximately proportional to the particle size, $d_d \propto 2r_d$. We claim that the image was well focused, after comparing it with images showing particles not well contoured, which we deemed as poorly focused. This simple technique can be used to estimate the size of single or just a few particles at a time clearly visible in the recorded images.

More complicated sizing techniques based on Mie scattering rely on the observation of interference fringes within the visible spot of a particle (Graßmann and Peters 2004). To evidence the variation of intensity with the scattering angle, an image with a sufficient high resolution is expected. In the case of small particles of 1 μm, other difficulties may arise, such as pixel locking or dependence of particle position (and diameter) on image focusing (Feng et al. 2007). These issues need be resolved for reliable results, especially when tracking of a large number of particles is performed. Finally, another situation that prevents the measurement of particle size is the overlapping of several dust particles in a given image.

https://doi.org/10.1017/S0022377812000967 Published online by Cambridge University Press

10. Conclusions

Dust in plasmas is emerging as an important field of research and is continuously enlarging its frontiers from fundamental science to applications in low-temperature plasmas as well as in fusion plasmas. Undoubtedly, high-speed imaging plays an essential role in the diagnostics and characterization of this type of plasma. Some examples where fast cameras provide critical information for determining singular or collective dynamics of micron size dust particles have been presented. These include falling of dust particles, oscillatory motion of trapped particles inside the plasma sheath, propagation of dust waves within dust crystals, and tracking hypervelocity dust particles accelerated by plasma jets. All these cases have in common the use of the time-of-flight technique to infer dust speed and acceleration by measuring the distance traveled by the particles in a given period of time. More elaborate techniques based on collective dust tracking are needed to deduce wavelength and then group velocity of dust waves observed in plasma crystals. In the future more powerful optics combined with CCDs with superior resolution at high-speed frame rates will contribute to a more detailed description of dust dynamics, and possibly other theoretically studied phenomena, such as dust spinning, dust coagulation, or dust segmentation, will be detected in real time.

Acknowledgements

C.M.Ticoş acknowledges support provided by the Sectoral Operational Program Human Resources and Development (SOP HRD) financed from the European Social Fund, and by the Romanian Government under contract POSDRU/89/1.5/*S*/63700. D. Toader, M. L. Munteanu, A. Scurtu, and N. Banu were supported by the National Authority for Scientific Research (ANCS) from contract Nucleu-LAPLAS 2012.

References

Adrian, R. J. 1991 Particle-imaging techniques for experimental fluid mechanics. *Annu. Rev. Fluid Mech.* **23**, 261–304.

Arp, O., Block, D., Piel, A. and Melzer, A. 2004 Dust coulomb balls: three-dimensional plasma crystals. *Phys. Rev. Lett.* **93**(16), 165004–1/4.

Barkan, A, Merlino, R. L. and D'Angelo, N. 1995 Laboratory observation of the dust-acoustic wave mode. *Phys. Plasmas* **2**(10), 3563–3565.

Barnes, M. S., Keller, J. H., Forster, J. C., O'Neill, J. A. and Coultas, D. K. 1992 Transport of dust particles in glow-discharge plasmas. *Phys. Rev. Lett.* **68**(3), 313–316.

Block, D. and Melzer, A. 2010 Imaging diagnostics in dusty plasmas. In: *Introduction to Complex Plasmas* (ed. M. Bonitz, N. Horing and P. Ludwig). New York: Springer, pp. 135–153.

Boyle, W. S. and Smith, G. E. 1970 Charged coupled semiconductor devices. *Bell Syst. Tech. J.* **49**(4), 587–593.

Cavarroc, M., Mikikian, M., Tessier, Y., and Boufendi, L. 2008 Instabilities during the growth of dust successive generations in silane-based plasmas. *Phys. Plasmas* **15**(10), 103704–1/9.

Chu, J. H., Du, J.-B. and Lin, I. 1994 Coulomb solids and low-frequency fluctuations in RF dusty plasmas. *J. Phys. D: Appl. Phys.* **27**(2), 296–300.

Chu, J. H. and Lin, I. 1994 Direct observation of Coulomb crystals and liquids in strongly coupled RF dusty plasmas. *Phys. Rev. Lett.* **72**(25), 4009–4012.

Feng, Y., Goree, J. and Bin, L. 2007 Accurate particle position measurement from images. *Rev. Sci. Instrum.* **78**(5), 053704–1/10.

Flanagan, T. M. and Goree, J. 2010 Observation of the spatial grow of self-excited dust-density waves. *Phys. Plasmas* **17**(12), 123702–1/9.

Fortov, V. E., Nefedov, A. P., Torchinski, V. M., Molotkov, V. I., Khrapak, A. G., Petrov, O. F. and Volykhin, K. F. 1996 Crystallization of a dusty plasma in the positive column of a glow discharge. *J. Exp. Theor. Phys.* **64**(2), 86–91.

Graßmann, A. and Peters, F. 2004 Size measurement of very small spherical particles by MIE scattering imaging (MSI). *Part. Part. Syst. Charact.* **21**, 374–389.

Harvey, P., Durniak, C., Samsonov, D. and Morfill, G. 2010 Soliton interaction in a complex plasma. *Phys. Rev. E* **81**(5), 057401–1/4.

Hayashi, Y. 1999 Structure of a three-dimensional Coulomb crystal in a fine-particle plasma. *Phys. Rev. Lett.* **83**(23), 4764–4767.

Heinrich, J., Kim, S.-H. and Merlino, R. L. 2009 Laboratory observations of self-excited dust acoustic shocks. *Phys. Rev. Lett.* **103**(11), 115002–1/4.

Himpel, M., Buttenschön, B. and Melzer, A. 2011 Three-view stereoscopy in dusty plasmas under microgravity: a calibration and reconstruction approach. *Rev. Sci. Instrum.* **82**(5), 053706–1/9.

Hutchinson, I. H. 2005 Ion collection by a sphere in a flowing plasma: 3. Floating potential and drag force. *Plasma Phys. Control. Fusion* **47**(1), 71–87.

Ikezi, H. 1986 Coulomb solid of small particles in plasma. *Phys. Fluids* **29**, 1764–1766.

Kennedy, R. V. and Allen, J. E. 2003 The floating potential of spherical probes and dust grains. ii: Orbital motion theory. *J. Plasma Phys.* **69**(6), 485–506.

Khrapak, S. A., Ivlev, A., Morfill, G. E. and Thomas, H. M. 2002 Ion drag in complex plasmas. *Phys. Rev. E* **66**(4), 046414–1/4.

Kong, J., Hyde, T. W., Matthews, L., Qiao, K., Zhang, Z. and Douglass, A. 2011 One-dimensional vertical dust strings in a glass box. *Phys. Plasmas* **84**(1), 016411–1/7.

Kurimoto, Y., Matsuda, N., Uchida, G., Iizuka, S., Suemitsu, M. and Sato, N. 2004 Fine particle removal by a negatively charged fine particle collector in silane plasma. *Thin Solid Films* **457**(2), 285–291.

Lapenta, G. 2002 Nature of the force field in plasma wakes. *Phyis. Rev. E* **66**(2), 026409–1/4.

Law, D. A., Steel, W. H., Annaratone, B. M. and Allen, J. E. 1998 Probe-induced particle circulation in a plasma crystal. *Phys. Rev. Lett.* **80**(19), 4189–4192.

Layden, B., Couëdel, L., Samarian, A. A. and Boufendi, L. 2011 Residual dust charges in a complex plasma afterglow. *IEEE Trans. Plasma Sci.* **39**(11), 2764–2765.

https://doi.org/10.1017/S0022377812000967 Published online by Cambridge University Press

Lindken, R., Westerweel, J. and Wieneke, B. 2006 Stereoscopic micro particle image velocimetry. *Exp. Fluids* **41**(2), 161–171.

Mamun, A. A. and Shukla, P. K. 2011 Discoveries of waves in dusty plasmas. *J. Plasma Phys.* **77**(4), 437–455.

Melzer, A. 2001 Laser manipulation of particles in dusty plasmas. *Plasma Sources Sci. Technol.* **10**(2), 303–310.

Melzer, A., Homann, A. and Piel, A. 1996 Experimental investigation of the melting transition of the plasma crystal. *Phys. Rev. E* **53**(3), 2757–2766.

Merlino, R. L., Barkan, A., Thompson, C. and D'Angelo, N. 1997 Experiments on waves and instabilities in dusty plasmas. *Plasma Phys. Control. Fusion* **39**, A421–A429.

Nichols, J. et al. 2011 3-D reconstruction of pre-characterized lithium and tungsten dust particle trajectories in NSTX. *J. Nucl. Mater.* **415**, S1098–S1101.

Oxtoby, N. P., Ralph, J. F., Durniak, C. and Samsonov, D. 2012 Tracking shocked dust: state estimation for a complex plasma during a shock wave. *Phys. Plasmas* **19**(1), 013708–1/10.

Piel, A., Arp, O. and Klindworth, M. 2008 Obliquely propagating dust-density waves. *Phys. Rev. E* **77**(2), 026407–1/7.

Pieper, J. B., Goree, J. and Quinn, R. A. 1996 Experimental studies of two-dimensional and three-dimensional structure in a crystallized dusty plasma. *J. Vac. Sci. Technol.* **14**, 519–524.

Rao, N. N., Shukla, P. K. and Yu, M. Y. 1990 Dust-acoustic waves in dusty plasmas. *Planet. Space Sci.* **38**(4), 543–546.

Roquemore, A. L., Nishino, N., Skinner, C. H., Bush, C., Kaita, R., Maqueda, R., Davis, W., Pigarov, S. H., Yu, A. and Krasheninnikov, S. I. 2007 3D measurements of mobile dust particle trajectories in NSTX. *J. Nucl. Mater.* **363–365**, 222–226.

Rosenberg, M. 1996 Ion dust streaming instability in processing plasmas. *J. Vac. Sci. Technol. A* **14**(2), 631–633.

Rudakov, D. L. et al. 2008 Dust measurements in tokamaks. *Rev. Sci. Instrum.* **79**(10), 10F303–1/6.

Samarian, A. A., James, B. W., Vladimirov, S. V. and Cramer, N. F. 2001 Self-excited vertical oscillations in an RF-discharge dusty plasma. *Phys. Rev. E* **64**(2), 025402(R)–1/4.

Samarian, A. A., Vladimirov, S. V. and James, B. W. 2005 Dust particle alignments and confinement in a radio frequency sheath. *Phy. Plasmas* **12**(2), 022103–1/6.

Samsonov, D., Goree, J., Thomas, H. M. and Morfill, G. E. 2000 Mach cone shocks in a two-dimensional Yukawa solid using a complex plasma. *Phys. Review E* **6**(5), 5557–5572.

Schill, R. A., Jr. 2002 A simplistic plasma dust removal model employing radiation pressure. *Laser Part. Beams* **20**(2), 341–357.

Shukla, P. K. and Eliasson, B. 2011 Colloquium: nonlinear collective interactions in quantum plasmas with degenerate electron fluids. *Rev. Mod. Phys.* **83**(3), 885–906.

Shukla, P. K. and Mamun, A. A. 2002 Introduction. In: *Introduction to Dusty Plasma Physics*. Bristol, UK: Institute of Physics, pp. 1–35.

Sütterlin, K. R. et al. 2009 Dynamics of lane formation in driven binary complex plasmas. *Phys. Rev. Lett.* **102**(8), 085003–1/4.

Thomas, E., Jr. 2001 Observations of high speed particle streams in dc glow discharge dusty plasmas. *Phys. Plasmas* **8**(1), 329–333.

Thomas, H. M. and Morfill, G. 1997 The processes involved in the solid to liquid phase transition. *Endeavour* **21**(4), 148–153.

Thomas, H., Morfill, G. E., Demmel, V., Goree, J., Feuerbacher, B. and Möhlmann, D. 1994 Plasma crystal: Coulomb crystallization in a dusty plasma. *Phys. Rev. Lett.* **73**(5), 652–655.

Thomas, E., Jr. and Williams, J. 2006 Applications of stereoscopic particle image velocimetry: dust acoustic waves and velocity space distribution functions. *Phys. Plasmas* **13**(5), 055702–1/6.

Ticos, C. M., Dyson, A. and Smith, P. W. 2004a The charge on falling dust particles in a RF discharge with DC negative bias. *Plasma Sources Sci. Technol.* **13**(3), 395–402.

Ticos, C. M., Dyson, A., Smith, P. W. and Shukla, P. K. 2004b Pressure triggered collective oscillations of a dust crystal in a capacitive RF plasma. *Plasma Phys. Control. Fusion* **46**, B293–B299.

Ticos, C. M., Jepu, I., Lungu, C. P., Chiru, P., Zaroschi, V. and Lungu, A. M. 2010a Levitated dust particles subjected to plasma jet. *J. Plasma Phy.* **76**(3–4), 501–511.

Ticos, C. M., Jepu, I., Lungu, C. P., Chiru, P., Zaroschi, V. and Lungu, A. M. 2010b Removal of floating dust in glow discharge using plasma jet. *Appl. Phys. Lett.* **97**(1), 011501–1/3.

Ticos, C. M., Smith, P. W. and Shukla, P. K. 2003 Experimental wake-induced oscillations of dust particles in a RF plasma. *Phys. Lett. A* **319**, 504–509.

Ticos, C. M., Smith, P. W. and Shukla, P. K. 2004c Oscillations of dust particles due to wake fields: an experimental demonstration. *Phys. Scr.* **T107**, 117–120.

Ticos, C. M., Wang, Z., Delzanno, G. L. and Lapenta, G. 2006a Plasma dragged microparticles as a method to measure plasma flows. *Phys. Plasmas* **10**(3), 103501–1/10.

Ticos, C. M., Wang, Z., Dorf, L. A. and Wurden, G. A. 2006b A plasma dynamic hypervelocity dust injector for the national spherical torus experiment. *Rev. Sci. Instrum.* **77**(10), 10E304–1/3.

Ticos, C. M., Wang, Z. and Wurden, G. A. 2011 Observation of the evolution of supersonic plasma jet launched by a coaxial gun. *IEEE Trans. Plasma Sci.* **39**(11), 2388–2389.

Ticos, C., Wang, Z., Wurden, G. A., Kline, J. L. and Montgomery, D. S. 2008a Plasma jet acceleration of dust particles to hypervelocities. *Phys. Plasmas* **15**(10), 103701–1/9.

Ticos, C. M., Wang, Z., Wurden, G. A., Kline, J. L., Montgomery, D. S., Dorf, L. A. and Shukla, P. K. 2008b Plasma drag acceleration of a dust cloud to hypervelocities. *Phys. Rev. Lett.* **100**(15), 155002–1/4.

Trottenberg, T., Melzer, A. and Piel, A. 1995 Measurement of the electric charge on particulates forming Coulomb crystals in the sheath of a radio-frequency plasma. *Plasma Sources Sci. Technol.* **4**(3), 450–458.

Uchida, G., Iizuka, S. and Sato, N. 2009 Liquid-crystal phase transition by electron shower in a direct current complex plasma. *Phys. Plasmas* **16**(8), 083707–1/6.

Wang, Z., Ticos, C. M., Dorf, L. A. and Wurden, G. A. 2006 Micro-particle probes for laboratory plasmas. *IEEE Trans. Plasma Sci.* **34**(232), 111–222.

https://doi.org/10.1017/S0022377812000967 Published online by Cambridge University Press

Wang, Z., Ticos, C. M. and Wurden, G. A. 2007 Dust trajectories and applications in plasmas beyond strongly coupled laboratory dusty plasmas. *Phys. Plasmas* **14**(10), 103701–1/11.

Willert, C. E. and Gharib, M. 1991 Digital particle image velocimetry. *Exp. Fluids* **10**(4), 181–193.

Williams, J. D. 2011 Application of tomographic particle image velocimetry to studies of transport in complex (dusty) plasma. *Phy. Plasmas* **18**(5), 050702–1/4.

Williams, J. D. and Thomas, E. D., Jr. 2007 Measurement of the kinetic dust temperature of a weakly coupled dusty plasma. *Phys. Plasmas* **14**(6), 063702–1/8.

https://doi.org/10.1017/S0022377812000967 Published online by Cambridge University Press